Reversible electron spirals by chirped attopulses at zero time delay

N. J. Strandquist, Jr. and J. M. Ngoko Djiokap

Reversible electron spiral by chirped attopulses at zero time delay

N.J. Strandquist, Jr[1] and J.M. Ngoko Djiokap[1]

[1]*Department of Physics and Astronomy, University of Nebraska, Lincoln, Nebraska 68588-0299, USA*

(Dated: September 27, 2022)

A novel class of linear, spiral phenomena is discovered in the photoelectron momentum distribution when studying photoionization of S-state atoms by a pair of linearly chirped, oppositely circularly polarized attosecond pulses eventually delayed in time by τ. This controllable effect, dubbed *reversible* electron spirals because of its energy-dependent sense of rotation, is identified and can be isolated in the absence of time delay for the case of opposite chirp rates. The astrophysical concept of spiral arm pitch angle is borrowed to gain a better insight into the energy-dependence of the reversible spiral rotation, to determine the attochirp as well as the binding energy characteristic of an atomic target. Our results indicate potential applications in attochirpmetry and polarimetry.

I. INTRODUCTION

A significant area of concern regarding the groundbreaking role of attosecond pulses [1–8] in achieving the ultimate goals [9] of attoscience is the compensation of their intrinsic chirp (known as attochirp) [10–13]. Indeed, current techniques for producing such coherent ultrashort light sources within the XUV or soft X-ray spectral region from high-order harmonic generation [1–7] or free-electron laser [8] always introduce a chirp, i.e., a time-dependent carrier frequency; this broadens their duration and decreases their intensity. Thus, for better control of electron motion (a main goal of attoscience), it is crucial to investigate how attochirp influences the photoelectron momentum distributions (PMDs).

Chirp as a control knob and its applications have been the subject of a variety of theoretical [14–31] and experimental [14, 22, 23, 28, 29, 31, 32] ionization studies in atoms, molecules [14, 23, 29, 31, 32], and condensed matter [26]; but mostly in femtosecond [14, 16, 17, 19, 20, 22, 23, 25, 26, 28–32] rather than in the attosecond [15, 18, 21, 24, 27] regime. Focusing on the XUV attosecond regime, studies include for instance chirp-sensitive single and double electron energy spectra in two-photon double ionization of He [18, 27], and chirp-induced left-right emission of electron in between adjacent above-threshold ionization peaks for H in its ground state [21, 24]. All these studies, however, are for *nonlinear (in intensity) processes* (except [15]) by a single *linearly-polarized light pulse* (except [23]), not for a *linear process* as considered here, where *a pair of oppositely circularly-polarized (OCP) broadband pulses with zero time delay* is shown to lead to an uncharted reference pattern of attoscience.

It is not surprising that chirp effects on a *linear process*, such as the fundamental process of single-photon single ionization (dubbed photoionization) from a state (not from a coherent superposition of electronic states as in [15]), have never been examined. This is so because for a single pulse, the chirp [24] or carrier-envelope phase (CEP) [21] has no effect within the rotating wave approximation (RWA), i.e., for negligible photoemission processes, see e.g., Fig. 4(a) or 4(b) in [30]. As demonstrated here by our prediction from perturbation theory (PT) analysis and confirmed numerically by our *ab initio* time-dependent Schrödinger equation (TDSE) calculations [33, 54, 55], this conclusion changes dramatically when a second pulse eventually delayed in time is brought into the game, with the two co-propagating pulses being OCP. This scheme for unchirped pulses (known as transform limited pulses or TLPs) with zero and nonzero time-delay is known to yield a dipole pattern and a two-arm Archimedean spiral (coined hereafter *irreversible* spiral) [33], respectively. Our discoveries [33] for one-photon, extended to single-color and two-color multiphoton ionization [34] have been confirmed experimentally [35–38] and opened up an interdisciplinary area in physics for searches and applications of this wave property of matter for different processes, targets, and regimes (see for instance [39–50]). Whether and how these two charted patterns of attoscience are changed by the experimentally tunable chirp needs to be elucidated.

In this contribution, we examine photoionization of an S-state atom (with binding energy E_b) within the RWA by a pair of linearly chirped OCP attopulses with central frequency ω_0 and eventually delayed in time by τ. Our findings are threefold. (i) For a pair of pulses with identical chirps, the PMDs at any τ coincide with those from TLPs; hence, the chirp has no effect. They exhibit dipole patterns for $\tau = 0$, and two-arm Archimedean spirals for $\tau \neq 0$ thanks to the linear (in energy) Ramsey [59] phase, $(E + E_b)\tau$, accumulated between the creation of the two continuum electronic wave packets. For these *irreversible* spirals, once the direction of this winding is established by the pulse helicities it is impossible to reverse it. (ii) The situation changes dramatically when the two chirp rates are equal with opposite signs, $\xi \equiv \xi_1 = -\xi_2$. For $\tau = 0$, instead of a dipole pattern, a *reversible* two-start spiral emerges in the PMD with its energy-dependent "handedness" given not only by the pulse helicities but also its chirp rate, which is our main finding. This exotic effect originates from the opposite signs for the linear and quadratic terms in the chirp-induced peculiar phase difference, $[(E + E_b) - \omega_0]^2 \tau_0^2 \xi$, between the two electronic wave packets created *simultaneously* in the continuum. It can thus be controlled by varying the chirp ξ, as well as

the duration (FWHM) τ_0 of the equivalent TLP. (iii) We introduce the astrophysical concept of pitch angle [51, 52] to determine the attochirp and get a better insight into the concepts of reversible versus irreversible spirals. Our predictions from a time domain physical picture based on an electric field analysis and a frequency domain physical picture based on first-order time-dependent PT analysis, are demonstrated numerically by *ab initio* TDSE simulations.

This paper is organized as follows. In Sec. II our parameterization of the chirped OCP attopulses is briefly described. In Sec. III we present our analytical and numerical results for the PMD for the cases where the two chirp rates are either identical or equal with opposite signs. In particular, Sec. III A is devoted to the predictions of the shape of the PMDs based on electric field analyses. These predictions for irreversible spirals from identical chirped OCP pulses and reversible spirals from oppositely chirped OCP pulses are demonstrated respectively in Secs. III B and III C. They are explained in Sec. III D by means of the concept of spiral arm pitch angle. In Sec. IV a brief summary of our results is provided. In Appendix A, we analyze for the time-dependence of the electric field for the pair of chirped OCP pulses. Meanwhile, a derivation for the ionization probability (4) for identically chirped pulses and ionization probability (5) for oppositely chirped pulses is presented in Appendix B. Atomic units (a.u.) are used throughout the text unless otherwise specified.

II. PARAMETRIZATION OF CHIRPED OPPOSITELY CIRCULARLY POLARIZED ATTOPULSES

We begin by parameterizing the electric field of a pair of elliptically-polarized, chirped attopulses delayed in time by τ as,

$$\mathbf{F}(t) = F_1(t) \, \mathrm{Re} \left\{ \mathbf{e}_1 e^{-i[\omega_1(t)t + \phi_{\mathrm{CE},1}]} \right\}$$
$$+ F_2(t - \tau) \, \mathrm{Re} \left\{ \mathbf{e}_2 e^{-i[\omega_2(t)(t-\tau) + \phi_{\mathrm{CE},2}]} \right\}, \quad (1)$$

where for the jth pulse ($j = 1, 2$) with CEP $\phi_{\mathrm{CE},j}$, $\mathbf{e}_j = (\hat{\varepsilon} + i\eta_j\hat{\zeta})/(1 + \eta_j^2)^{1/2}$ is the polarization vector, with $\hat{\varepsilon} \equiv \hat{x}$ and $\hat{\zeta} \equiv \hat{y}$ defining the major and minor axes of the polarization ellipse; and $|\eta_j|$ is the ellipticity, where $-1 \leq \eta_j \leq 1$ [53]: $|\eta_j| = 0$ for linear polarization, $|\eta_j| = 1$ for circular polarization (CP), and $\eta_j < 1$ for elliptical polarization. The sign of η_j defines the helicity; $\eta_j = +1(-1)$ defines right (left) circularly polarized pulse, abbreviated RCP (LCP). In Eq. (1), $F_j(t) = \sqrt{I_j} \exp(-2\ln 2 \frac{t^2}{\tau_j^2})$ is the Gaussian envelope. Here, the peak intensity $I_j = I_0/(1 + \xi_j^2)^{1/2}$ and duration $\tau_j = \tau_0(1 + \xi_j^2)^{1/2}$ are modified by the chirp rate ξ_j [24], which is positive (up-chirp) or negative (down-chirp). Note that $I_0 = F_0^2$, τ_0, and ω_0 are respectively the peak intensity, duration (FWHM) of the intensity

profile, and central carrier frequency of the equivalent TLP. The dimensionless chirp rate ξ_j can be manipulated by other means as described in [9] or by propagating the pulse through dispersive media with thickness d_j and group velocity dispersion (GVD) k_j'', where $\phi_j'' = k_j'' d_j \equiv \xi_j \tau_0^2/(4\ln 2)$ [28, 56, 58] is the group delay dispersion (GDD) [28, 56–58]. Since chirp extends the effective pulse duration, the peak intensity is correspondingly reduced to maintain equivalent total energy with the chirp-free pulse. This allows for a clear comparison between the chirped and chirp-free cases. The linearly chirped instantaneous frequency is

$$\omega_j(t) = \omega_0 + 2\ln 2 \frac{\xi_j}{1 + \xi_j^2} \frac{t}{\tau_0^2} \equiv \omega_0 + b_j t. \quad (2)$$

Throughout this work, $\omega_0 = 36$ eV and all other pulse parameters (except the chirp) are identical between the pulses (see the caption of Fig. 1), barring only the fact that the second pulse may be delayed in time. Below, two cases are considered depending on the chirp: $\xi_1 = \xi_2$ or $b_1 = b_2$ for identically chirped pulses, and $\xi \equiv \xi_1 = -\xi_2$ or $b \equiv b_1 = -b_2$ for oppositely chirped pulses.

III. ANALYTICAL AND NUMERICAL RESULTS

In the following, we provide a physical picture in both the time and frequency domains on whether reversible versus irreversible spirals occur in the PMD. Section III A is devoted to a time domain physical picture, where our predictions are based on the time-dependence of the electric field of chirped OCP pulses. Meanwhile, Secs. III B and III C provide a frequency domain physical picture based on the first-order PT analysis, which explains all the findings from TDSE calculations.

A. Predictions of the shape of the PMDs based on electric field analyses

For photoionization of an $^1\mathrm{S}^e$ atomic state, the pair of chirped or unchirped attopulses separated in time by τ (see, e.g., Fig. 4 where $\tau = 2$ fs) produce a pair of $^1\mathrm{P}^o$ continuum electron wave packets (EWPs), which spread out owing to dispersion and interfere [59]. However, in contrast to TLPs where the phase difference Φ accumulated between the birth of the two EWPs involves the Ramsey phase $(E + E_b)\tau$ and the CEP difference $\phi_{\mathrm{CE},12} \equiv \phi_{\mathrm{CE},1} - \phi_{\mathrm{CE},2}$ [33], the chirped nature of the attopulses may introduce an additional peculiar phase difference, whose effects on the PMD are very different from these two phase difference components. To demonstrate this and isolate this peculiar chirp-induced phase difference, let us inspect Figs. 1(a,b) showing $F_x(t)$ and $F_y(t)$ at zero time delay and CEPs, for which the Ramsey phase and $\phi_{\mathrm{CE},12}$ vanish. For identically chirped OCP
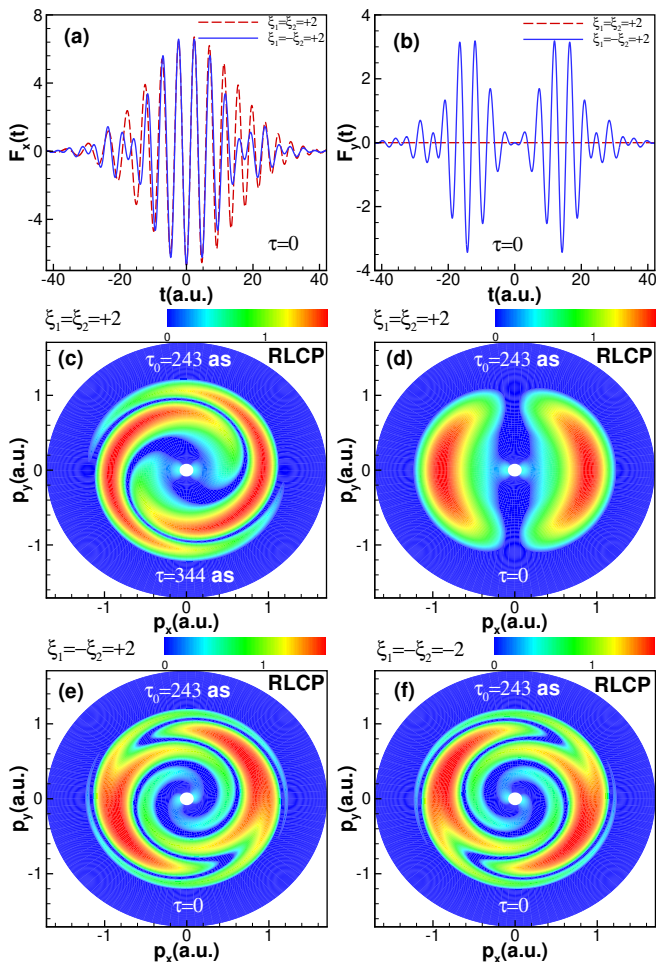
FIG. 1. Top: Chirp-dependence of the x-component (a) and y-component (b) of $\mathbf{F}(t)$ (1) for two OCP pulses at a zero time delay, $\tau = 0$. Middle and Bottom: TDSE results for PMD in the polarization plane produced by a pair of RLCP chirped attopulses, with CEPs $\phi_{CE,1} = \phi_{CE,2} = 0$, for the case of equal chirp rates $\xi_1 = \xi_2 = +2$ for (c) $\tau = \sqrt{2}\tau_0$ and (d) $\tau = 0$; and the case of opposite chirp rates with (e) $\xi_1 = -\xi_2 = +2$ and (f) $\xi_1 = -\xi_2 = -2$ for $\tau = 0$. Parameters of the corresponding Gaussian TLP are: a central frequency $\omega_0 = 36$ eV, duration (FWHM) $\tau_0 = 243$ as, and intensity $I_0 = 100$ TW/cm^2. All results for the PMD and electric field components are in units of 10^{-2} a.u.

pulses, $\omega_1(t)$ and $\omega_2(t)$ defined by (2) vary at the same rate; thus, $F_{1,x}(t)$ and $F_{2,x}(t)$ add up constructively to yield in Fig. 1(a) an intense burst of light for $F_x(t)$, while $F_{1,y}(t)$ and $F_{2,y}(t)$ cancel out to yield $F_y(t) = 0$ as shown in Fig. 1(b). Hence, the total electric field $\mathbf{F}(t)$ at $\tau = 0$ becomes linearly polarized along the x-axis, leading to a dipole pattern in the PMD as exemplified by the TDSE result in Fig. 1(d) for $\xi_1 = \xi_2 = +2$. As this result for identically chirped pulses is similar to TLPs, such a scheme (in contrast to oppositely chirped pulses) does not give rise to the peculiar phase difference and *PMDs by identically chirped pulses and TLPs are expected to coincide.*

For oppositely chirped OCP pulses at $\tau = 0$, $\omega_j(t)$ defined by (2) rises or falls linearly as time flies for up-chirp or down-chirp. The corresponding optical period $2\pi/\omega_j(t)$ decreases or increases with time. Consequently, positive and negative optical interference between $F_{1,x}(t)$ and $F_{2,x}(t)$ yields a single burst of light for $F_x(t)$ as exemplified by Fig. 1(a) for $\xi = +2$, while Fig. 1(b) reveals a surprising pair of light bursts well separated in time for $F_y(t)$. *This unique temporal structure in $F_y(t) \propto F_1(t)\cos(\omega_0 t + \phi_{CE,1})\sin(bt^2)$ with a chirp-induced effective time delay from $\sin(bt^2)$ [60] suggests that the PMDs from oppositely and identically chirped pulses differ.* However, since the spectral phase of the burst of light is directly mapped in the continuum electron, the use of first-order PT appears as a natural analytical tool to extract the exact expression for this peculiar phase. Indeed, within a PT framework [60] we find that this peculiar phase $\propto [\omega_0 - (E + E_b)]^2\tau_0^2\xi_j$ with a linear dependence in chirp and a quadratic dependence in energy and TLP duration (FWHM), is directly mapped out in $\hat{F}_j^+(\epsilon)$ (where $\epsilon \equiv E + E_b$), the positive-frequency component of the Fourier transform of the pulse describing photoabsorption processes [24]:

$$\hat{F}_j^+(\epsilon) = F_0\tau_0\sqrt{\frac{\pi}{16\ln 2}}\frac{\sqrt{1 - i\xi_j}}{(1 + \xi_j^2)^{1/4}}$$

$$\times \exp\left[-\frac{\tau_0^2}{16\ln 2}(\omega_0 - \epsilon)^2(1 - i\xi_j)\right]. \quad (3)$$

Below, for identically or oppositely chirped OCP pulses we use PT and TDSE calculations to demonstrate the two above expectations based on electric field analyses.

B. Irreversible electron spirals produced by identical chirped OCP pulses

For the case $\xi_1 = \xi_2$ of OCP attopulses delayed in time by τ, $\hat{F}_1^+(\epsilon) = \hat{F}_2^+(\epsilon)$. The triply differential probablity (TDP), $\mathcal{W}(\mathbf{p})$, derived in [60] can be written as:

$$\mathcal{W}(\mathbf{p}) = g(p)\sin\theta\cos^2(\Phi/2 - \hat{\eta}\varphi), \quad (4)$$

where $\mathbf{p} \equiv (p, \theta, \varphi)$ is the photoelectron momentum $\mathbf{p}$; $\Phi \equiv (E + E_b)\tau + \phi_{CE,12}$; $\hat{\eta} = +1(-1)$ for RLCP (LRCP); and the dynamical real parameter, $g(p) = I_0\tau_0^2(\pi/8\ln 2)|\Upsilon(p)|^2\exp[-\tau_0^2(\omega_0 - \epsilon)^2/(8\ln 2)]$, only depends on energy $E \equiv p^2/2$, not on angles. Here, $\Upsilon(p) \equiv \Upsilon_j(p)$ is the radial matrix element between the ground state and final state. Critically, one sees that the chirp is absent from the TDP (4) when the two pulses have the same chirp. This expression is identical to earlier results for TLPs (unchirped pulses) [33], in which the τ-dependence of the TDP from OCP pulses is ultimately responsible for the formation of two-arm spiral patterns in the PMD in the polarization plane ($\theta = \pi/2$). All these PT predictions correlate well with our TDSE results, as the PMD in Fig. 1(c) for $\xi_1 = \xi_2 = +2$ coincides with the

PMDs for $\xi_1 = \xi_2 = -2$ (not shown) and for any value of equal chirps, including the chirp-free case. While other pulse parameters are specified in the caption of Fig. 1, the time delay here is $\tau = \tau_0 = 243$ as, corresponding to 3 cycles for a central frequency $\omega_0 = 36$ eV well above the ionization threshold in He ($E_b = 24.6$ eV). For our Gaussian pulse, the bandwidth (FWHM) for a TLP calculated from $\tau_0(\mathrm{as})\Delta\omega(\mathrm{eV}) \approx 1825$ is $\Delta\omega = 7.5$ eV, meaning that the chirp-sensitive Rydberg levels in He are not accessible. For $\tau = 0$, the TDP (4) predicts a dipole pattern whose direction is dictated by $\Phi = \phi_{\mathrm{CE},12}$. As $\phi_{\mathrm{CE},12} = 0$ in Fig. 1(d), the dipole pattern is along the major x-axis.

C. Reversible electron spirals by oppositely chirped OCP pulses

For the case $\xi \equiv \xi_1 = -\xi_2$ of OCP pulses, $\hat{F}_1^+(\epsilon) = \hat{F}_2^{+*}(\epsilon)$ and the TDP in the polarization plane is [60]:

$$\mathcal{W} = g(p)\cos^2\left[(\Phi+\beta)/2 - \frac{\tau_0^2(\omega_0-\epsilon)^2\xi}{16\ln 2} - \hat{\eta}\varphi\right]. \quad (5)$$

The TDPs (4) and (5) have the same structure, with the only difference being the presence of a chirp-induced phase shift $\beta = \tan^{-1}(\xi)$ in the kinematical factor, together with the peculiar phase $\propto [\omega_0 - (E+E_b)]^2\tau_0^2\xi$, stemming from the phase of $\hat{F}_j^+(\epsilon)$ in (3). This is particularly significant, because this basic quadratic phase in energy is independent of the time delay. This suggests that helical patterns similar to spirals [33] may be observed without the second pulse being delayed in time, which is impossible for TLPs and identically chirped pulses.

Equations describing the pattern that emerges in the in-plane PMD are determined by zeros and maxima of the argument of the cosine factor in the TDP (5):

$$\varphi^{\mathrm{max},0}(E) = \hat{\eta}\left\{k\pi + (\Phi+\beta)/2 - \frac{\tau_0^2(\omega_0-\epsilon)^2\xi}{16\ln 2}\right\}, \quad (6)$$

where k is an integer for maxima and half-integer for zeros. For $\xi \neq 0$, setting $\tau = 0$ allows us to isolate, access, and measure the novel attochirp-induced helical spiral pattern (our main finding) which is described by Eqs. (5) and (6), and whose energy-dependent handedness is defined not only by $\hat{\eta}$ but also by the sign of the attochirp ξ. For RLCP, i.e., $\hat{\eta} = +1$ our TDSE results for the PMD are shown in Fig. 1(e) for $\xi = +2$ and Fig. 1(f) for $\xi = -2$. First, one sees clearly that these two patterns in the polarization plane are mirror images of each other. We found (not shown) that using $\hat{\eta} = -1$ (LRCP) with ξ unchanged swaps the patterns in Fig. 1(e) and Fig. 1(f). Second, each spiral pattern in those two figures has two starts since one photon is absorbed from each of the two pulses. Third, the handedness of those spirals is energy-dependent (see, e.g., Fig. 1(e)) where the counterclockwise spirals observed for low energy become clockwise for high energy; they are dubbed *reversible* spirals. This is in contrast to *irreversible* electron spirals produced by
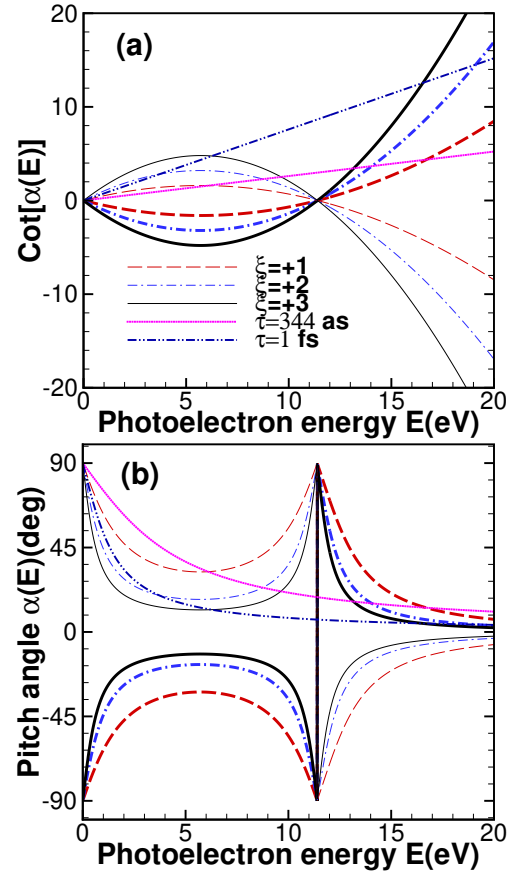

FIG. 2. Variation with energy E of the pitch angle (b) and its cotangent (a) at $\tau = 0$ for six values of the attochirp: $\xi = \pm 1$ [long-dashed red thin (+) and thick (-) line], ± 2 [dash-dotted blue thin (+) and thick (-) line], and ± 3 [solid black thin (+) and thick (-) line]. Also shown are results for TLPs for two values of the time delay: $\tau = \sqrt{2}\tau_0 = 344$ as (dotted magenta line), and $3\sqrt{2}\tau_0$ (dash double-dotted purple line).

OCP TLPs [33] or identically chirped pulses [see, e.g., Fig. 1(c)] where once the direction of a spiral winding is established by $\hat{\eta}$, it is impossible to reverse it.

The origin of this energy-dependent spiral handedness at $\tau = 0$ and $\xi \neq 0$ can be understood qualitatively from the expansion: $(\omega_0-\epsilon)^2\tau_0^2\xi = (\omega_0^2 - 2\omega_0\epsilon + \epsilon^2)\tau_0^2\xi$ in Eq. (5). Just as with $\phi_{\mathrm{CE},12}$ or $\beta = \tan^{-1}(\xi)$ in the TDP (5), the first term $\omega_0^2\tau_0^2\xi$ in this expansion induces a global rotation of the PMD in Fig. 1(e). For a fixed ξ and $\hat{\eta}$, since τ_0^2 is positive definite, the linear $-2\omega_0\epsilon\tau_0^2\xi$ and quadratic $\epsilon^2\tau_0^2\xi$ terms in energy with opposite sign will rotate the dipole pattern to generate spirals in two opposite directions. However, while the linear term $-2\omega_0\epsilon\tau_0^2\xi$ dictates the spiral handedness at low energy, the quadratic term $\epsilon^2\tau_0^2\xi$ dominates at high energy.

D. Spiral arm pitch angle for attochirpmetry

To not only determine the attochirp ξ but also gain a quantitatively better insight into this E-dependence of

the reversible spiral handedness, we introduce the astrophysical concept of spiral arm pitch angle $\alpha(E)$. It is the angle between the tangents of a spiral arm and of a perfect circle of radius E [51, 52]. This angle, defined by $\cot\alpha(E) = E[\partial\varphi(E)/\partial E]$ [52], can be obtained from the spiral equation (6) for zeros and maxima, $\varphi^{\max,0}(E)$ as:

$$\cot\alpha(E) = E\tau/2 + E[\omega_0 - (E + E_b)](\tau_0^2/8\ln 2)\xi. \quad (7)$$

Plotted in Fig. 2(a) and Fig. 2(b) are TDSE results for $\cot\alpha(E)$ and $\alpha(E)$, respectively, for three positive (thin lines) and three negative (thick lines) values of ξ at $\tau = 0$. Details on different styles of curves are specified in the caption of Fig. 2, see also the legend of Fig. 2(a). For comparison, also displayed in these two panels of this figure are TDSE results for two values of τ for TLPs: $\tau = \sqrt{2}\tau_0 = 344$ as in dotted magenta lines, and $\tau = 3\sqrt{2}\tau_0$ in dash double-dotted purple lines. First, while $\cot\alpha(E)$ for TLPs varies linearly with τ as expected from PT Eq. (7), $\alpha(E)$ decreases monotonically or irreversibly with the energy E. The longer the time delay τ in Fig. 2(b), the faster the decrease in energy and the faster the irreversible spiral arms become tightly wound. Second, in concert with PT Eq. (7), the three fish-like shapes of $\cot\alpha(E)$ in Fig. 2(a) for oppositely chirped pulses at $\tau = 0$ vary linearly with ξ. This linear dependence suggests a trivial determination of the chirp from the pitch angle at any energy E. For measuring the pitch angle, one may use either well-established graphical methods [52] or direct extraction via numerical data processing as done here. In Fig. 2(b), $\alpha(E)$ exhibits a concave-up (concave-down) shape for up-chirp (down-chirp) for 0.1 eV $< E < E_c$ with an extremum at $E = E_c/2$, then change the sign at $E = E_c = \omega_0 - E_b$ when $\partial\varphi^{\max,0}(E)/\partial E = 0$, followed by a monotonically increase (decrease) toward zero for $E > E_c$. Hence, this shape of the pitch angle $\alpha(E)$ from TDSE results or PT (7), reflects the energy-dependent handedness of reversible spirals. Measuring E_c as a node in $\cot\alpha(E)$ provides a means to identify the target under investigation by determining its binding energy E_b.

Due to the phase $(\omega_0 - \epsilon)^2\tau_0^2\xi$ in the TDP (5), reversible spirals can be exquisitely controlled by varying ξ at fixed $\tau_0 = 243$ as and $\tau = 0$, see Figs. 3(a) and 3(b) for $\xi = +1$ and $+3$. Compared to Fig. 1(e) for $\xi = +2$, increasing the attochirp ξ leads to more windings in the two directions, with each one becoming tightly wound, see also the steeper walls and flatter bottom of the U-shaped valleys in Fig. 2(b) as ξ increases from 1 to 3. For an even better visualization of the dependence of this electron phenomenon on ξ, we provide an animation showing the evolution with the attochirp ξ in the range $0 \leq \xi \leq 3$ of the reversible spiral in the Supplemental Material [60].

Another effective knob to control this polarization effect is τ_0. For a fixed $\xi = +2$, Figs. 3(c) and 3(d) give the PMDs for $\tau_0 = 81$ as and 405 as by LRCP pulses. Compared to Fig. 1(d) for $\tau_0 = 243$ as and $\xi = -2$, it appears that while short τ_0 can lead to broader bandwidth, it may not be enough to produce reversible spi-
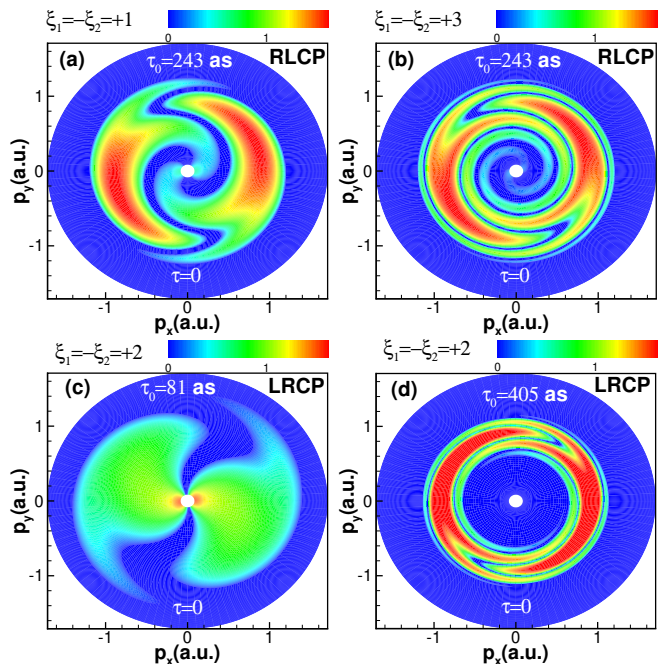

FIG. 3. Control of the two-arm reversible spiral displayed in Figs. 1(e,f) by varying the chirp rate (top), and the duration (FWHM) of the equivalent TLP τ_0 (bottom).

rals. In contrast, while longer τ_0 produces several windings, the rather small bandwidth leads to a tightly wound reversible spiral pattern that is almost circular.

IV. SUMMARY AND CONCLUSIONS

In summary, we have identified an experimentally accessible scheme where a novel class of electron matter-wave vortex spirals occurs. This linear and controllable phenomenon, called a reversible spiral, requires oppositely chirped and OCP pulses with zero time delay, and the broad bandwidth characteristic of attopulses. Whilst isolated attosecond pulses with full control of their polarization states exist [7], our predicted reversible spirals can be observed even using femtopulses [35–38], but in experiments with chirp control as in [22, 28]. The concept of pitch angle (7) introduced here in attoscience transparently explains the concept of reversible versus irreversible spirals, and can be used to fully determine the attochirp ξ, the time delay τ for TLPs if considered, and also identify the atomic system under investigation.

Appendix A: Electric field analyses

The x-component and y-component of the electric field $\mathbf{F}(t)$ in Eq. (1) for two OCP copropagating pulses delayed in time by τ can be written as,

$$F_{1,x}(t) = -\frac{F_1(t)}{\sqrt{1+\eta_1^2}}\cos[\omega_1(t)t + \phi_{\mathrm{CE},1}], \qquad (A1)$$

$$F_{1,y}(t) = -\frac{\eta_1 F_1(t)}{\sqrt{1+\eta_1^2}}\sin[\omega_1(t)t + \phi_{\mathrm{CE},1}], \qquad (A2)$$

$$F_{2,x}(t) = -\frac{F_2(t-\tau)}{\sqrt{1+\eta_2^2}}\cos[\omega_2(t)(t-\tau) + \phi_{\mathrm{CE},2}], \qquad (A3)$$

$$F_{2,y}(t) = -\frac{\eta_2 F_2(t-\tau)}{\sqrt{1+\eta_2^2}}\sin[\omega_2(t)(t-\tau) + \phi_{\mathrm{CE},2}], \qquad (A4)$$

where $\eta_1 = -\eta_2 = \pm 1$ are the ellipticies for OCP pulses, and $\omega_{1,2}(t) = \omega_0 + b_{1,2}t$ are the instantaneous frequencies of the first and second pulses, with $b_{1,2} \equiv 2\ln 2\,\xi_{1,2}/(1+\xi_{1,2}^2)\tau_0^2$. Here, $b_1 = b_2$ for the case (i): $\xi_1 = \xi_2$, and $b \equiv b_1 = -b_2$ for the case (ii): $\xi \equiv \xi_1 = -\xi_2$; and the Gaussian envelope functions $F_{1,2}(t)$ are defined below Eq. (1).

For a longer time delay $\tau = 2$ fs such that the two pulses almost do not overlap, while Fig. 4(a) for $F_x(t)$ and Fig. 4(b) for $F_y(t)$ present a similar temporal structure, they only differ by a $\pi/2$ out-of-phase due to cosine and sine functions for their carrier waves. As $\xi_1 = +2$ in cases (i) and (ii), the color of the first burst of light curve in both $F_x(t)$ and $F_y(t)$ is magenta (superposition of red and blue). It exhibits denser oscillations, characteristic of up-chirp spectrograms, since $\omega_1(t)$ and the corresponding optical period $2\pi/\omega_1(t)$ rises and decreases with time. As the second pulse is up-chirp for the case (i) and down-chirp for the case (ii), two different second light bursts appear in both $F_x(t)$ and $F_y(t)$, see thick red long dashed lines for the case (i) and thin blue solid lines for the case (ii). As $\omega_2(t)$ and $2\pi/\omega_2(t)$ respectively falls and increases as time flies, the second burst of light for the case (ii) exhibits lesser oscillations, characteristic of down-chirp spectrograms.

For $\tau = 0$, optical interference takes place: Figs. 1(a) and 1(b) for $F_x(t)$ and $F_y(t)$ support this. For the case (i), $\omega_1(t)$ and $\omega_2(t)$ are equal and they vary at the same rate; thus, constructive interference between $F_{1,x}(t)$ (A1) and $F_{2,x}(t)$ (A3) occurs, yielding $F_x(t)$ with a double field strength if $\phi_{\mathrm{CE},1} = \phi_{\mathrm{CE},2}$, as shown in Fig. 1(a). As $\eta_1 = -\eta_2 = \pm 1$, Eqs. (A2) and (A4) show that $F_y(t) = F_{1,y}(t) + F_{2,y}(t) = 0$, see Fig. 1(b).

Still for $\tau = 0$ but for the case (ii), while $\omega_1(t)$ for up-chirp rises with time, $\omega_2(t)$ for down-chirp decreases with time. Consequently, positive and negative interference between $F_{1,x}(t)$ (A1) and $F_{2,x}(t)$ (A3) takes place and yields a single light burst for $F_x(t)$, see Fig. 1(a). The same effect between $F_{1,y}(t)$ (A2) and $F_{2,y}(t)$ (A4) occurs, which strikingly results to a pair of time-delayed bursts of light in $F_y(t)$, see Fig. 1(b). Indeed, these shapes for $F_x(t)$ and $F_y(t)$ for $\phi_{\mathrm{CE},1} = \phi_{\mathrm{CE},2}$ becomes clear
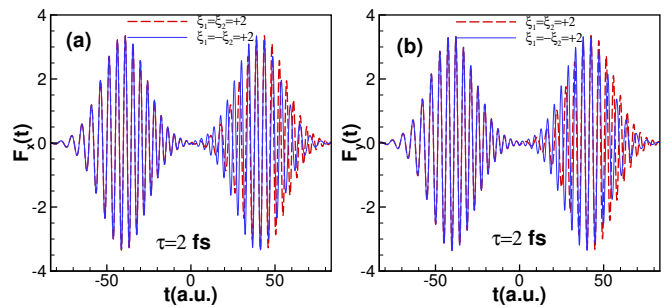

FIG. 4. Chirp-dependence of $F_x(t)$ and $F_y(t)$ in units of 10^{-2} a.u. for two OCP pulses at time delay $\tau = 2$ fs. Other pulse parameters are the same as in Fig. 1.

when they are expressed analytically by adding either $F_{1,x}(t)$ and $F_{2,x}(t)$ defined by (A1) and (A3) or $F_{1,y}(t)$ and $F_{2,y}(t)$ defined by (A2) and (A4):

$$F_x(t) = -\sqrt{2}F_1(t)\cos(\omega_0 t + \phi_{\mathrm{CE},1})\cos(bt^2), \qquad (A5)$$

$$F_y(t) = -\sqrt{2}F_1(t)\cos(\omega_0 t + \phi_{\mathrm{CE},1})\sin(bt^2). \qquad (A6)$$

With the same chirp-dependent envelope $F_1(t)$ and chirp-independent carrier wave $\cos(\omega_0 t + \phi_{\mathrm{CE},1})$, one sees that $F_x(t)$ and $F_y(t)$ are shaped differently by the chirp-dependent terms $\cos(bt^2)$ and $\sin(bt^2)$ because of the two different instantaneous carrier frequencies, as illustrated below.

From the green dotted curves in Fig. 5(a) for $\xi = +2$, one sees that the flat-top shape of $\cos(bt^2)$ for $-7 \le t \le 7$ a.u. keeps unchanged the pulse $F_1(t)\cos(\omega_0 t + \phi_{\mathrm{CE},1})$, while its oscillatory structure occurring outside this time window interferes with this pulse and changes it from regular to irregular oscillatory structures for $|t| > 7$ a.u. This fully explains the temporal structure observed for $F_x(t)$ and represented by the blue curve in Fig. 1(a).

Meanwhile, the concave-up pattern of $\sin(bt^2)$ for $\xi = +2$ [see blue solid curves in Fig. 5(a)] present for $-25 \le t \le 25$ a.u. does interfere with the pulse $F_1(t)\cos(\omega_0 t + \phi_{\mathrm{CE},1})$, and strongly transforms it from a single burst to a pair of light bursts well separated in time for $F_y(t)$, see Fig. 1(b). To see how this effective time delay builds up with the chirp, Figs. 5(c) and 5(d) compare $F_y(t)$ for the reference $\xi = +2$ with two other values $\xi = +1, +3$. Clearly, increasing b results in broadening the effective time delay, see plots of $\sin(bt^2)$ in Fig. 5(a) as ξ changes from $+1$ to $+3$.

From the chirp definition $b \equiv 2\ln 2\,\xi/(1+\xi^2)\tau_0^2$, it is trivial that $\sin(bt^2)$ for ξ and $1/\xi$ coincide, as illustrated in Fig. 5(a) for $\xi = +2$ (blue solid lines) and $\xi = +0.5$ (black long dashed lines). However, Fig. 5(b) shows that the pair of time-delayed bursts of light emerging in $F_y(t)$ from the case (ii) for fixed ξ and $1/\xi$ differ. This difference highlights the role played by the Gaussian envelope $F_1(t)$ in shaping $F_y(t)$, since small ξ leads to taller Gaussian envelope $F_1(t) = F_0/(1+\xi^2)^{1/4}\exp(-2\ln 2t^2/(1+\xi^2)\tau_0^2)$ with smaller width.
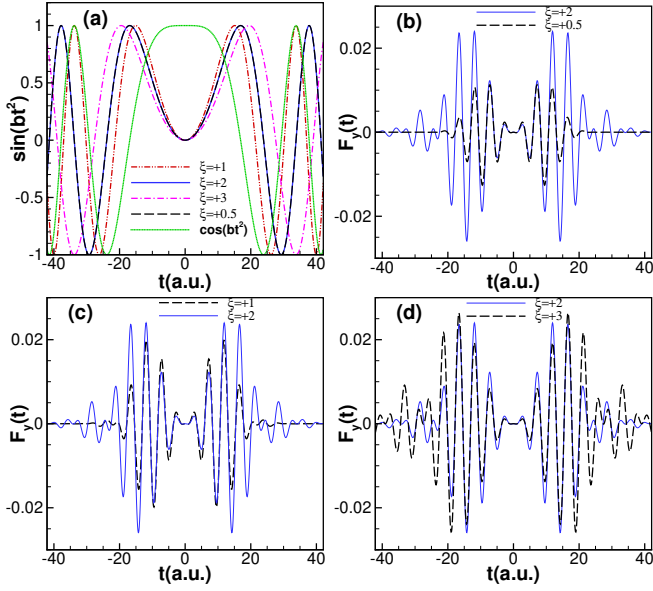
FIG. 5. (a) Time-dependence of (a) the chirp-induced window function $\sin(bt^2)$ for four values of chirp rate: $\xi = +0.5, +1, +2, +3$. Shown also for comparison is $\cos(bt^2)$ for $\xi = +2$. Panels (b)-(d): Comparison between the temporal structure of $F_y(t)$ for two OCP pulses at $\tau = 0$ for (b) $\xi = +2$ and $\xi = +0.5$, (b) $\xi = +2$ and $\xi = +1$, and (b) $\xi = +2$ and $\xi = +3$. The chirp-induced effective time delay between the two light bursts in (b)-(d) increases with $\xi \equiv \xi_1 = -\xi_2$.

Appendix B: First-order PT analysis for a derivation of Eqs. (4) and (5)

For a negligible spin-orbit coupling and within the electric dipole approximation, the first-order transition amplitude for one-photon single ionization of S-state atoms (with binding energy E_b) produced by the electric field pulse, $\mathbf{F}(t)$ defined by Eq. (1), is [33, 61]:

$$\mathcal{A} = -i \int_{-\infty}^{+\infty} e^{iE_f t} \langle \Psi_{\nu,\mathbf{p}}^{(-)}|[\mathbf{d} \cdot \mathbf{F}(t)]|i\rangle e^{-iE_i t} dt, \quad \text{(B1)}$$

where $\mathbf{d}$ is the electric dipole moment operator of the atom; $|i\rangle$ and $|\Psi_{\nu,\mathbf{p}}^{(-)}\rangle$ denote the initial and final states with energy E_i and E_f; and $\epsilon \equiv E_f - E_i$. For pulse intensity below 10^{14} W/cm^2, the RWA is valid, i.e., the c.c. part of $\mathbf{F}(t)$ in (B1) is negligible. It is convenient to parameterize the amplitude (B1) – weighted by $e^{-i\phi_{\mathrm{CE},1}}$ – in terms of kinematical and dynamical components [53]:

$$\mathcal{A} = [\Upsilon_1(p)\hat{F}_1^+(\epsilon)(\mathbf{e}_1 \cdot \hat{\mathbf{p}}) + \Upsilon_2(p)\hat{F}_2^+(\epsilon)(\mathbf{e}_2 \cdot \hat{\mathbf{p}})e^{i\Phi}], \quad \text{(B2)}$$

where $\Phi = (E + E_b)\tau + (\phi_{\mathrm{CE},1} - \phi_{\mathrm{CE},2})$ and the chirp is encoded in $\hat{F}_1^+(\epsilon)$, see Eq. (3). Using Eq. (B2) to calculate the TDP, $\mathcal{W} = |\mathcal{A}|^2$, one gets:

$$\mathcal{W} = |\Upsilon(p)|^2 \left\{ |\hat{F}_1^+(\epsilon)|^2|\mathbf{e}_1 \cdot \hat{\mathbf{p}}|^2 + |\hat{F}_2^+(\epsilon)|^2|\mathbf{e}_2 \cdot \hat{\mathbf{p}}|^2 \right.$$
$$\left. +2\,\mathrm{Re}\,[\hat{F}_1^{+*}(\epsilon)\hat{F}_2^+(\epsilon)(\mathbf{e}_1^* \cdot \hat{\mathbf{p}})(\mathbf{e}_2 \cdot \hat{\mathbf{p}})e^{i\Phi}] \right\}, \quad \text{(B3)}$$

which is valid for any light polarization for both case (i) where $\xi_1 = \xi_2$ and case (ii) where $\xi \equiv \xi_1 = -\xi_2$; and assumes negligible ground state depletion, i.e., $\Upsilon(p) \equiv \Upsilon_1(p) \simeq \Upsilon_2(p)$ for the radial matrix elements. For OCP attopulses, $(\mathbf{e}_1 \cdot \hat{\mathbf{p}}) = (\mathbf{e}_2^* \cdot \hat{\mathbf{p}}) = \sin\theta \, \exp(i\hat{\eta}\varphi)/\sqrt{2}$, where θ and φ are the spherical angles of $\mathbf{p}$, and $\hat{\eta} = +1$ for right-left circularly polarized (RLCP) and -1 for left-right circularly polarized(LRCP) pulses.

For the case $\xi_1 = \xi_2$ of OCP attopulses, $\hat{F}_1^+(\epsilon) = \hat{F}_2^+(\epsilon)$, meaning that $|\hat{F}_1^+(\epsilon)|^2$ appears as a global factor in (B3). Its evaluation using Eq. (3) shows that it is chirp-independent. Using $|\mathbf{e}_j \cdot \hat{\mathbf{p}}|^2 = (1/2)\sin^2\theta$ for $j = 1, 2$ and $(\mathbf{e}_1^* \cdot \hat{\mathbf{p}})(\mathbf{e}_2 \cdot \hat{\mathbf{p}}) = (1/2)\sin^2\theta \exp(-2i\hat{\eta}\varphi)$ together with some trigonometry identities, the calculated TDP (B3) leads easily to Eq. (4).

For the case $\xi \equiv \xi_1 = -\xi_2$ of OCP pulses, $\hat{F}_1^+(\epsilon) = \hat{F}_2^{+*}(\epsilon)$, meaning that it is the cross term $\propto \hat{F}_1^{+*}(\epsilon)\hat{F}_2^+(\epsilon)$ in (B3) that gives a chirp dependence to the TDP. After some manipulations using trigonometry identities, the TDP (B3) leads easily to Eq. (5), where $\mathbf{p}$ is detected in the polarization plane.

[1] P.M. Paul, E.S. Toma, P. Breger, G. Mullot, F. Augé, Ph. Balcou, H.G. Muller, and P. Agostini, "Observation of a train of attosecond pulses from high harmonic generation," Science **292**, 1689 (2001).

[2] M. Hentschel, R. Kienberger, C. Spielmann, G.A. Reider, N. Milosevic, T. Brabec, P. Corkum, U. Heinzmann, M. Drescher, and F. Krausz, "Attosecond Metrology," Nature **414**, 509-513 (2001).

[3] G. Sansone, E. Benedetti, F. Calegari, C. Vozzi, L. Avaldi, R. Flammini, L. Poletto, P. Villoresi, C. Altucci, R. Velotta, S. Stagira, S. De Silvestri, and M. Nisoli, "Isolated Single-Cycle Attosecond Pulses," Science **314**, 443-446 (2006).

[4] E. Goulielmakis, M. Schultze, M. Hofstetter, V.S. Yakovlev, J. Gagnon, M. Uiberacker, A.L. Aquila, E.M. Gullikson, D.T. Attwood, R. Kienberger, F. Krausz, and

U. Kleineberg, "Single-Cycle Nonlinear Optics," Science **320**, 1614-1617 (2008).

[5] S. Gilbertson, Y. Wu, S.D. Khan, M. Chini, K. Zhao, X. Feng, and Z. Chang, "Isolated Attosecond Pulse Generation Using Multicycle Pulses Directly from a Laser Amplifier," Phys. Rev. A **81**, 043810 (2010).

[6] K. Zhao, Q. Zhang, M. Chini, Y. Wu, X. Wang, and Z. Chang, "Tailoring a 67 Attosecond Pulse Through Advantageous Phase- Mismatch," Opt. Lett. **37**, 3891-3893 (2012).

[7] P.-C. Huang, C. Hernández-García, J.-T. Huang, P.-Y. Huang, C.-H. Lu, L. Rego, D.D. Hickstein, J.L. Ellis, A. Jaron-Becker et al., "Polarization control of isolated high-harmonic pulses," Nature Photon. **12**, 349 (2018).

[8] J. Duris, S. Li, T. Driver, E.G. Champenois, J.P. MacArthur, A.A. Lutman, Z. Zhang, P. Rosenberger,

J.W. Aldrich, R. Coffee et al., "Tunable isolated attosecond X-ray pulses with gigawatt peak power from a free-electron laser," Nature Photon. **14**, 30 (2020).

[9] M. Nisoli, P. Decleva, F. Calegari, A. Palacios, and F. Martín, "Attosecond electron dynamics in molecules," Chem. Rev. **117**, 10760 (2017).

[10] K.T. Kim, C.M. Kim, M.-G. Baik, G. Umesh, and C.H. Nam, "Single sub-50-attosecond pulse generation from chirp-compensated harmonic radiation using material dispersion," Phys. Rev. A **69**, 051805(R) (2004).

[11] R. López-Martens, K. Varjú, P. Johnsson, J. Mauritsson, Y. Mairesse, P. Salières, M.B. Gaarde, K.J. Schafer, A. Persson, S. Svanberg, C.-G. Wahlström, and A. L'Huillier, "Amplitude and Phase Control of Attosecond Light Pulses," Phys. Rev. Lett. **94**, 033001 (2005).

[12] F. Frassetto, P. Villoresi, and L. Poletto, "Optical Concept of a Compressor for XUV Pulses in the Attosecond Domain," Opt. Express **16**, 6652-6667 (2008).

[13] L. Poletto, P. Villoresi, E. Benedetti, F. Ferrari, S. Stagira, G. Sansone, and M. Nisoli, "Intense Femtosecond Extreme Ultraviolet Pulses by Using a Time-Delay-Compensated Monochromator," Opt. Lett. **32**, 2897-2899 (2007).

[14] D. Mathur, and F.A. Rajgara, "Dissociative ionization of methane by chirped pulses of intense laser laser light," J. Chem. Phys. **120** 5616 (2004).

[15] G.L. Yudin, A.D. Bandrauk, and P.B. Corkum, "Chirped Attosecond Photoelectron Spectroscopy," Phys. Rev. Lett. **96**, 063002 (2006).

[16] T. Nakajima, "Above-threshold ionization by chirped laser pulses," Phys. Rev. A **75**, 053409 (2007).

[17] T. Nakajima and E. Cormier, "Effects of the carrier-envelope phase of chirped laser pulses in the multiphoton ionization regime," Opt. Lett. **32**, 2879 (2007).

[18] T.-G. Lee, M.S. Pindzola, and F. Robicheaux, "Energy and angular differential probabilities for photoionization of He using chirped attosecond soft-x-ray pulses," Phys. Rev. A **79**, 053420 (2009).

[19] M. J. Abel, T. Pfeifer, A. Jullien, P.M. Nagel, M. J. Bell, D. M. Neumark, and S. R. Leone, "Carrier-envelope phase-dependent quantum interferences multiphoton ionization," J. Phys. B **42**, 075601 (2009).

[20] Y. Xiang, Y. Niu, and S. Gong, "Above-threshold ionization by few-cycle nonlinear chirped pulses," Phys. Rev. A **80**, 023423 (2009).

[21] L.-Y. Peng, F. Tan, Q. Gong, E.A. Pronin, and A.F. Starace, "Few-cycle attosecond pulse chirp effects on asymmetries in ionized electron momentum distributions," Phys. Rev. A **80**, 013407 (2009).

[22] M. Krug, T. Bayer, M. Wollenhaupt, C. Sarpe-Tudoran, T. Baumert, S.S. Ivanov, and N.V. Vitanov, "Coherent strong-field control of multiple states by a single chirped femtosecond laser pulse," New J. Phys. **11**, 105051 (2009).

[23] P. Horsch, G. Urbasch, K.-M. Weitzel, and D. Kröner, "Circular dichroism in ion yields employing femtosecond laser ionization – the role of the laser pulse duration," Phys. Chem. Chem. Phys. **13**, 2378 (2011).

[24] E.A. Pronin, A.F. Starace, and L.-Y. Peng, "Perturbation-theory analysis of ionization by a chirped few-cycle attosecond pulse," Phys. Rev. A **84**, 013417 (2011).

[25] S. Laulan, J. Hache, H.S. Ba, and S. Barmaki, "Ionization process of atoms by intense femtosecond chirped laser pulses," J. Mod. Phys. **4**, 20-26 (2013).

[26] J.R. Gulley, and T.E. Lanier, "Model for ultrashort laser pulse-induced ionization dynamics in transparent solids," Phys. Rev. B **90**, 155119 (2014).

[27] S. Barmaki, P. Lanteigne, and S. Laulan, "Control of two-photon double ionization of helium with intense chirped attosecond laser pulses," Phys. Rev. A **89**, 063406 (2014).

[28] D. Zille, D. Adolph, M. Möller, A.M. Sayler, and G.G. Paulus, "Chirp and carrier-envelope-phase effects in the multiphoton regime: measurements and analytical modeling o strong-field ionization of sodium," New J. Phys. **20**, 063018 (2018).

[29] B. Kaufman, T. Rozgonyi, P. Marquetand, and T. Weinacht, "Competition between dynamic resonance and internal conversion in strong-field molecular ionization with chirped ultrafast laser pulses," Phys. Rev. A **103**, 023108 (2021).

[30] F. Zhu, X. Liu, Y. Gao, N. Wang, L. Jiao, A. Liu, "Chirp-dependent ionization of hydrogen atoms in the presence of super-intense laser pulses," Chin. Phys. B **30**, 0944209 (2021).

[31] S. Li, B. Jochim, J. Stamm, D. Peng, H.-C. Shao, J.M. Ngoko Djiokap, and M. Dantus, "Pulse shaping in strong-field ionization: theory and experiments," Submitted to Phys. Rev. A (under review).

[32] V. Schäfer, and K.-M. Weitzel, "Qualitative and quantitative distinction of ortho-, meta-, and para-fluorescence by means of chirped femtosecond laser ionization," Anal. Chem. **92**, 5492 (2020).

[33] J.M. Ngoko Djiokap, S.X. Hu, L.B. Madsen, N.L. Manakov, A.V. Meremianian, and A.F. Starace, "Electron vortices in photoionization by circularly polarized attosecond pulses," Phys. Rev. Lett. **115**, 113004 (2015).

[34] J.M. Ngoko Djiokap, A.V. Meremianin, N.L. Manakov, S.X. Hu, L.B. Madsen, and A.F. Starace, "Multistart spiral electron vortices in ionization by circularly polarized UV pulses," Phys. Rev. A **94** 013408 (2016).

[35] D. Pengel, S. Kerbstadt, D. Johannmeyer, L. Englert, T. Bayer, and M. Wollenhaupt, "Electron vortices in femtosecond multiphoton ionization," Phys. Rev. Lett. **118**, 053003 (2017).

[36] D. Pengel, S. Kerbstadt, L. Englert, T. Bayer, and M. Wollenhaupt, "Control of three-dimensional electron vortices from femtosecond multiphoton ionization," Phys. Rev. A **96**, 043426 (2017).

[37] S. Kerbstadt, K. Eickhoff, T. Bayer, and M. Wollenhaupt, "Odd electron wave packets from cycloidal ultrashort laser fields," Nat. Comm. **10**, 658 (2019).

[38] S. Kerbstadt, K. Eickhoff, T. Bayer, and M. Wollenhaupt, "Control of free electron wave packets by polarization-tailored ultrashort bichromatic laser fields," Advances in Physics: X **4**, 1672583 (2019).

[39] K.-J. Yuan, S. Chelkowski, and A. D. Bandrauk, "Photoelectron momentum distributions of molecules in bichromatic circularly polarized attosecond UV laser fields," Phys. Rev. A **93**, 053425 (2016).

[40] K.-J. Yuan, H. Lu, and A. D. Bandrauk, "Photoionization of triatomic molecular ions H_3^{2+} by intense bichromatic circularly polarized attosecond UV laser pulses," J. Phys. B **50**, 124004 (2017).

[41] J.M. Ngoko Djiokap, A.V. Meremianin, N.L. Manakov, S.X. Hu, L.B. Madsen, and A.F. Starace, "Kinematical vortices in double photoionization of helium by attosecond pulses," Phys. Rev. A. **96**, 013405 (2017).

[42] J.M. Ngoko Djiokap and A.F. Starace, "Doubly-excited state effects on two-photon double ionization of helium by time-delayed, oppositely circularly-polarized attosecond pulses," J. Opt. **19**, 124003 (2017).

[43] Z.L. Li, Y. J. Li, and B. S. Xie, "Momentum vortices on pairs production by two counter-rotating fields," Phys. Rev. D **96**, 076010 (2017).

[44] M. Li, G. Zhang, T. Zhao, X. Ding, and J. Yao, "Electron vortices in photoionization by a pair of elliptically polarized attosecond pulses," Chinese Opt. Lett. **15**, 120202 (2017).

[45] M. Li, G. Zhang, X. Kong, T. Wang, X. Ding, and J. Yao, "Dynamic Stark induced vortex momentum of hydrogen in circular fields," Opt. Express **26**, 878 (2018).

[46] X. Kong, G. Zhang, M. Li, T. Wang, X. Ding, and J. Yao, "Odd-fold-symmetric spiral momentum distributions and their Stark distortions in hydrogen," J. Opt. Soc. Am. B **35**, 2163 (2018).

[47] J.M. Ngoko Djiokap, A.V. Meremianin, N.L. Manakov, L.B. Madsen, S.X. Hu, and A.F. Starace, "Dynamical electron vortices in attosecond double photoionization of H$_2$," Phys. Rev. A **98**, 063407 (2018).

[48] X.-R. Xiao, M.-X. Wang, H. Liang, Q. Gong, and L.-Y. Peng, "Proposal for measuring electron displacement induced by a short laser pulse," Phys. Rev. Lett. **122**, 053201 (2019).

[49] L. Geng, F. Cajiao Vélez, J.Z. Kamiński, L.-Y. Peng, and K. Krajewska, "Vortex structures in photodetachment by few-cycle circularly polarized pulses," Phys. Rev. A **102**, 043117 (2020).

[50] J.M. Ngoko Djiokap, "Atomic photoionization by multiple temporal pairs of slits," Phys. Rev. A **104**, 013115 (2021).

[51] J. Binney and S. Tremaine, "Galactic dynamics," 2nd Ed.; Princeton, NJ: Princeton Univ. Press, (2008).

[52] S.-Y. Yu and L.C. Ho, "On the connection between spiral arm pitch angle and galaxy properties," The Astrophysical Journal **871**, 194 (2019).

[53] E.A. Pronin, A.F. Starace, M.V. Frolov, and N.L. Manakov, "Perturbation theory analysis of attosecond photoionization," Phys. Rev. A **80**, 063403 (2009).

[54] J.M. Ngoko Djiokap, N.L. Manakov, A.V. Meremianin, S.X. Hu, L.B. Madsen, and A.F. Starace "Nonlinear dichroism in back-to-back double ionization of He by an intense elliptically polarized few-cycle extreme ultraviolet pulse," Phys. Rev. Lett. **113**, 223002 (2014).

[55] J. M. Ngoko Djiokap, S. X. Hu, W.-C. Jiang, L.-Y. Peng, and A. F. Starace, "Enhanced asymmetry in few-cycle attosecond pulse ionization of He in the vicinity of autoionizing resonances," New J. Phys. **14**, 095010 (2012).

[56] T. Csizmadia, L.G. Oldal, P. Ye, S. Majorosi, P. Tzallas, G. Sansone, V. Tosa, K. Varjú, B. Major, and S. Kahaly, "Detailed study of quantum path interferences in high harmonic generation driven by chirped laser pulses," New J. Phys. **23**, 123012 (2021).

[57] M. Wollenhaupt, A. Assion, and T. Baumert, "Femtosecond Laser Pulses: Linear Properties, Manipulation, Generation and Measurement," Springer Handbook of Laser and Optics, Chapter 12, (2007).

[58] Z. Chang, "Fundamentals of Attosecond Optics," Boca Raton, FL: CRC Press (2011).

[59] N. F. Ramsey, "A molecular beam resonance method with separated oscillating fields," Phys. Rev. **78**, 695 (1950).

[60] See Supplemental Material at [URL will be inserted by publisher] for an animation of the evolution of the reversible spiral with the attochirp. The range over which ξ varies is $0 \le \xi \le 3$ and pulse parameters are the same pulse as in Fig. 1(e). In the animation, eight values of the attochirp ξ are used in this range: $\xi(0) = 0$, $\xi(1) = 0.5$, $\xi(2) = 0.75$, $\xi(3) = 1$, $\xi(4) = 1.5$, $\xi(5) = 2$, $\xi(6) = 2.5$, and $\xi(7) = 3$.

[61] A.S. Davydov, "Quantum Mechanics," 2nd Ed. (Pergamon Press, Oxford, 1976).